Observation of a Multimode Plasma Response and its Relationship to Density Pumpout and Edge-Localized Mode Suppression

C. Paz-Soldan,[1,*] R. Nazikian,[2] S. R. Haskey,[3] N. C. Logan,[2] E. J. Strait,[1] N. M. Ferraro,[1] J. M. Hanson,[4] J. D. King,[1] M. J. Lanctot,[1] R. A. Moyer,[5] M. Okabayashi,[2] J-K. Park,[2] M. W. Shafer,[6] and B. J. Tobias[2]

[1]*General Atomics, San Diego, California 92121, USA*

[2]*Princeton Plasma Physics Laboratory, Princeton, New Jersey 08543, USA*

[3]*Plasma Research Laboratory, Australian National University, Canberra, Australian Capital Territory 0200, Australia*

[4]*Columbia University, New York, New York 10027, USA*

[5]*University of California, San Diego, 9500 Gilman Drive, La Jolla, California 92093-0417, USA*

[6]*Oak Ridge National Laboratory, P.O. Box 2008, Oak Ridge, Tennessee 37831-6169, USA*

(Received 15 October 2014; published 12 March 2015)

Density pumpout and edge-localized mode (ELM) suppression by applied $n = 2$ magnetic fields in low-collisionality DIII-D plasmas are shown to be correlated with the magnitude of the plasma response driven on the high-field side (HFS) of the magnetic axis but not the low-field side (LFS) midplane. These distinct responses are a direct measurement of a multimodal magnetic plasma response, with each structure preferentially excited by a different $n = 2$ applied spectrum and preferentially detected on the LFS or HFS. Ideal and resistive magneto-hydrodynamic (MHD) calculations find that the LFS measurement is primarily sensitive to the excitation of stable kink modes, while the HFS measurement is primarily sensitive to resonant currents (whether fully shielding or partially penetrated). The resonant currents are themselves strongly modified by kink excitation, with the optimal applied field pitch for pumpout and ELM suppression significantly differing from equilibrium field alignment.

DOI: 10.1103/PhysRevLett.114.105001 PACS numbers: 52.30.Cv, 52.35.Py, 52.55.Fa, 52.55.Tn

Introduction and motivation.—The simultaneous control of transiently large heat loads while maintaining high thermal confinement is essential in future fusion reactors. However, instabilities such as edge-localized modes (ELMs) can lead to unacceptable levels of wall erosion in a burning plasma experiment such as ITER unless these loads can be substantially mitigated [1]. One approach for ELM mitigation and suppression is the use of non-axisymmetric (three-dimensional, 3D) magnetic fields, a technique which has been demonstrated on several facilities [2–5].

Applied 3D fields are thought to impact ELM stability through their resonant components, defined as the $m = nq$ harmonics at rational surfaces, where (m, n) is the (poloidal, toroidal) harmonic and q is the local safety factor. Resonant components can either drive shielding currents along the field line (preserving good flux surfaces), or alternatively, shielding can be imperfect thus allowing the formation of magnetic islands. $n > 1$ fields can also modify particle exhaust and significantly reduce the plasma density, a phenomenon termed density pumpout [6]. 3D fields of all n also excite weakly stable pressure-driven kink modes [7–11], which are here explicitly defined as the amplification of the $m > nq$ harmonics at all surfaces. Kink excitation has been critical to understanding $n = 1$ error field correction [12–14] (where n is toroidal mode number). In contrast, its function in $n > 1$ density pumpout and ELM suppression has remained unclear, as has the role of the plasma response more generally. As kink excitation is sensitive to particular equilibrium properties, basic understanding of its role in pumpout and ELM suppression is an essential element of a predictive model for either phenomenon.

On the DIII-D tokamak, $n = 2$ fields are well suited to experimentally measure this connection. Recent work has shown that $n = 2$ fields can suppress ELMs [15], yet unlike with $n = 3$ the relative $n = 2$ phase between in-vessel coil rows can be continuously varied on DIII-D, thus allowing experimental access to a broader range of poloidal spectra than with $n = 3$ [16]. Recent upgrades to the magnetic probe suite on DIII-D also allow direct measurement of $n = 2$ responses on both the tokamak low-field side (LFS) and high-field side (HFS) midplanes [17].

In this Letter, we continuously vary the applied $n = 2$ poloidal spectrum to show that pumpout and ELM suppression are correlated with the amplitude of the magnetic plasma response measured near the HFS midplane. In contrast, the LFS midplane response is most excited by an $n = 2$ applied spectrum different than that which most excites the HFS, directly demonstrating the presence of multiple structures in the response. We generically refer to these structures as "modes," though their relationship to the eigenmodes of the magneto-hydrodynamic (MHD) equations is still under study. Further, while the MHD equations are inherently multimodal, the excitability by applied fields and importance to the plasma sensitivity of multiple modes is unclear. Additionally, no direct observation of a multimode response is found in the literature. Linear MHD simulations are here used to connect the multimode

observations to a pressure-driven kink mode and resonant currents. Kink mode excitation will be shown to be correlated with the LFS response but not with pumpout or ELM suppression, while the resonant currents will be shown to be correlated with the HFS response and indeed with pumpout and ELM suppression. Note that as the kink structure extends beyond $m > nq$ to $m = nq$, the kink and resonant currents are coupled. Probe measurements as well as pumpout and ELM suppression are found to be maximized for applied field pitches distinct from equilibrium field alignment, illustrating the importance of the plasma response to all observable effects.

This Letter is structured as follows. The experimental setup is first described, with emphasis on the nonaxisymmetric coil configuration used. The axisymmetric plasma ($n = 0$) response is then described and compared to ideal-MHD modeling of global plasma response metrics. The connection to the measured $n = 2$ magnetic plasma response follows, where experimental data combined with ideal and resistive MHD modeling allow the separation of the multimode response into contributions from resonant currents and kink mode excitation.

Experimental setup.—These discharges are configured as ITER-similar-shape plasmas, with plasma current (I_p) of 1.37 MA, toroidal field (B_T) of 1.94 T, minor radius (a) of 0.6 m, internal inductance (l_i) of 1.0, neutral beam injected power of 6 MW, modest electron cyclotron resonance heating of 1 MW, yielding a normalized electron pedestal collisionality (ν_e^*) of 0.23. The value of the edge safety factor (q_{95}) of 4.1 in these discharges is a half-integer above the previous $n = 2$ ELM suppression window [15]. The in-vessel coils are configured such that the lower in-vessel coil row is fixed in toroidal phase (ϕ_{IL}), while the upper row toroidal phase (ϕ_{IU}) can be continuously rotated. Scanning only ϕ_{IU} yields a continuous scan in upper-lower phase difference ($\Delta\phi_{\mathrm{UL}} \equiv \phi_{\mathrm{IU}}$-$\phi_{\mathrm{IL}}$), thus scanning the applied $n = 2$ poloidal spectrum. The applied $n = 2$ also contains $n = 4$ sidebands, though these are substantially smaller and are not considered [16]. While continuous toroidal rotation of arbitrary $\Delta\phi_{\mathrm{UL}}$ is not presently possible due to hardware limitations, polarity inversions (termed phase flips) at arbitrary $\Delta\phi_{\mathrm{UL}}$ are permitted and utilized to directly measure the nonaxisymmetric component of the plasma response. Note ϕ_{IU} and ϕ_{IL} are defined such that for a coil at a given toroidal angle ϕ_{coil}, its current is proportional to $\cos(n\phi_{\mathrm{coil}} - \phi_{\mathrm{IU,IL}})$.

A typical discharge evolution is shown in Fig. 1. The $n = 2$ field is energized with initial $\Delta\phi_{\mathrm{UL}} = 0°$, and after an initial equilibration time $\Delta\phi_{\mathrm{UL}}$ is scanned at 1 Hz. Figure 1(c) illustrates the large modulation in global ($n = 0$) plasma parameters, such as the pedestal density ($n_{e,\mathrm{ped}}$) and normalized pressure (β_N). Brief periods of ELM suppression are repeatedly found at the $n_{e,\mathrm{ped}}$ minima, centered at about $\Delta\phi_{\mathrm{UL}} = 30°$.

Throughout this work, the DIII-D ex-vessel coils are used to apply $n = 1$ and $n = 2$ intrinsic error field correction. $n = 2$ currents were determined experimentally by finding the ex-vessel currents that eliminated the modulation of the $n = 0$ response when the toroidal phase of the in-vessel field was scanned at fixed $\Delta\phi_{\mathrm{UL}}$. To assess the role of any residual $n = 2$ error fields after ex-vessel correction, $\Delta\phi_{\mathrm{UL}}$ scans with shifted ϕ_{IL} were performed. The phase shift in ϕ_{IL} yielded a phase shift of the $n = 0$ response vs ϕ_{IU} such that results in terms of $\Delta\phi_{\mathrm{UL}}$ were unchanged, thus confirming that residual error fields are not strongly influencing these results.

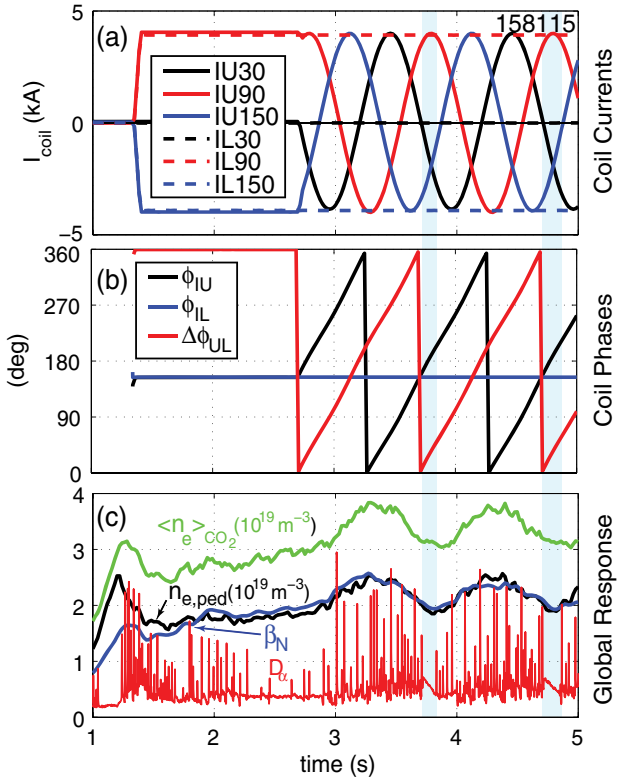

FIG. 1 (color online). Time-domain display of a typical discharge scanning $\Delta\phi_{\mathrm{UL}}$. (a) In-vessel coil currents and (b) toroidal phase of each coil row and phase difference ($\Delta\phi_{\mathrm{UL}}$). (c) Interferometer and pedestal density ($n_{e,\mathrm{ped}}$), normalized pressure (β_N), and divertor recycling light (D_α). Note brief periods of ELM suppression at the $n_{e,\mathrm{ped}}$ minima.

Axisymmetric plasma response.—As preluded in Fig. 1, axisymmetric ($n = 0$) plasma parameters are strongly modified by $\Delta\phi_{\mathrm{UL}}$. This information is summarized in Fig. 2. Density pumpout (indicated by $n_{e,\mathrm{ped}}$), energy confinement (indicated by β_N), and rotation braking (indicated by the total angular momentum L_ϕ) are all modulated in unison and indicate a maximum effect at $\Delta\phi_{\mathrm{UL}} \approx 30°$. The tight coupling of $n_{e,\mathrm{ped}}$ and β_N is consistent with the invariance of the pedestal electron temperature ($T_{e,\mathrm{ped}}$) as $\Delta\phi_{\mathrm{UL}}$ is scanned. The angular momentum may have a slight phase shift, though data quality prohibits identification of this subtle change. Figure 2(d) illustrates the brief periods of ELM suppression found at the same $\Delta\phi_{\mathrm{UL}}$ that maximizes the reduction of $n_{e,\mathrm{ped}}$. A bifurcation is found in the HFS magnetic response T_e and rotation profiles in the

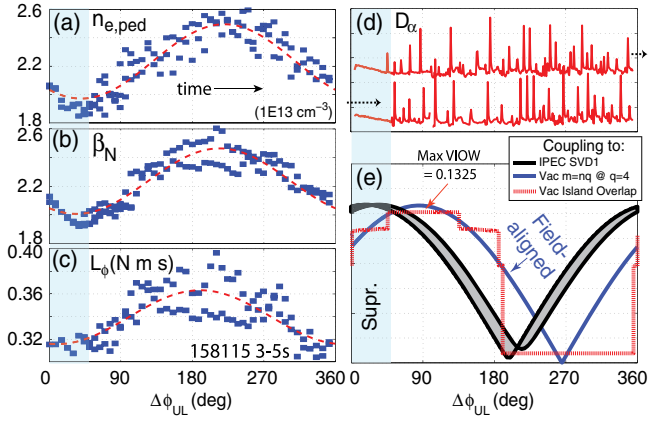

FIG. 2 (color online). [(a)–(d)] Effect on global ($n = 0$) plasma parameters as $\Delta\phi_{UL}$ is scanned through two periods. L_ϕ is the total angular momentum. (e) IPEC SVD1 coupling and comparison to equilibrium field alignment and vacuum island overlap width (VIOW).

narrow $\Delta\phi_{UL}$ window where ELM suppression occurs and is the focus of future work.

The $\Delta\phi_{UL}$ value corresponding to maximum pumpout and ELM suppression onset is found to be coincident with a maximum of the coupling of the $n = 2$ field to the resonant ($m = nq$) current coupling as calculated by the ideal perturbed equilibrium code (IPEC) [18]. To define a global metric for resonant current drive (formally, shielding current drive as IPEC is an ideal MHD code), IPEC calculates the coupling of external fields to each resonant surface and then performs a singular-value decomposition (SVD) on the coupling to all resonant surfaces to identify the optimal spectrum for coupling. Assuming strong singular value separation, the first SVD mode (SVD1) is a suitable global metric for resonant field drive. SVD1 coupling is shown in Fig. 2(e), illustrating that maximum resonant field coupling is coincident with maximum $n = 0$ effect. IPEC calculations are done using equilibrium reconstructions at both $n_{e,ped}$ extrema, illustrating weak sensitivity to kinetic profiles.

Maximal $n = 0$ effect is found at a different $\Delta\phi_{UL}$ than that which aligns with the equilibrium field line or maximizes vacuum island overlap width [19], shown in Fig. 2(e). Because of the invariance of the equilibrium field-line pitch with minor radius on the LFS, the same value of $\Delta\phi_{UL}$ aligns with the equilibrium field line on all rational surfaces simultaneously. That ELM suppression is found away from equilibrium field alignment illustrates the general importance of the plasma response to this phenomenon. This is also consistent with previous work that found wider $n = 2$ ELM suppression windows in q_{95} at lower $\Delta\phi_{UL}$ than equilibrium field alignment [15]. Previous work using $n = 3$ fields at fixed $\Delta\phi_{UL}$ of 0 or 180° found pumpout at certain I_p where the fixed $\Delta\phi_{UL}$ value was near field alignment [20]. Here, the ability to smoothly vary $\Delta\phi_{UL}$ resolves that while field-aligned $\Delta\phi_{UL}$ does drive more pumpout than $\Delta\phi_{UL} + 180°$, field-aligned $\Delta\phi_{UL}$ is not optimal.

Nonaxisymmetric plasma response.—Measurements and modeling indicate that two distinct modes of the $n = 2$ magnetic response are present and that the kink mode plays an indirect role in the $n = 0$ dynamics through the modification of the resonant currents. Experimental measurements are made by the novel technique of phase flips of an applied 4 kA $n = 2$ field at several finely spaced values of $\Delta\phi_{UL}$ within a single discharge. Note that $n_{e,ped}$ was elevated through gas puffing and ELM suppression was avoided throughout the phase flip scan. Figure 3 shows the measured $n = 2$ poloidal field component magnitude on the LFS (a) and HFS (b) midplane of the tokamak. These locations are chosen as they have very weak vacuum coupling to the in-vessel coils (regardless of $\Delta\phi_{UL}$) and thus allow robust signal extraction.

HFS and LFS sensors are found to have strikingly different dependencies on $\Delta\phi_{UL}$, a result that directly confirms the presence of multiple structures (or "modes") [21] to the response. Were there only one mode to be excited, its dependence on $\Delta\phi_{UL}$ would be consistent across the poloidal cross section. The response null in $\Delta\phi_{UL}$ would also be global and represent the spectrum that does not excite that mode. Instead, a phase shift of ≈90° is found between sensor arrays, providing direct identification of multiple plasma response modes at a single n. While only response magnitude is shown, the measured phase on both arrays rotates 180° as $\Delta\phi_{UL}$ goes around 360° and jumps 180° at the $\Delta\phi_{UL}$ null.

Synthetic diagnostics within the IPEC code capture the dependence of the probe signals to $\Delta\phi_{UL}$, as shown in Figs. 3(a) and 3(b). The computed IPEC response across the plasma cross-section confirms the more global nature of the HFS response null. At the LFS null [Fig. 3(c)], significant responses remain across most of the cross-section, while at the HFS null [Fig. 3(d)] only response fields at the LFS

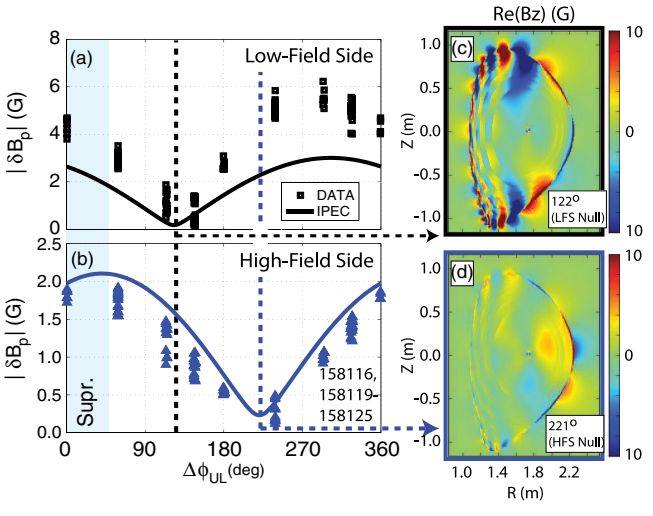

FIG. 3 (color online). Experimental $n = 2$ plasma response amplitude and IPEC modeling at the (a) LFS and (b) HFS midplane as $\Delta\phi_{UL}$ is stepped. Cross-section of the computed response at the LFS null (c) and HFS null (d).

remain. This calculation indicates that displacements at the X-points would also be expected to go like the HFS response, consistent with previous modeling that found a correlation in pumpout to the ratio of X-point displacements to LFS midplane displacements [22]. The modeling presented in Refs. [20,22] also predicts that different $n = 3$ response structures are excited by $\Delta\phi_{UL}$ of 0° rather than 180°, suggesting the multimode response is not unique to $n = 2$. Figure 3(c) shows that off-midplane LFS sensors could also identify the presence of multiple response modes. The agreement between probe signals and ideal-MHD computation also shows that perfect shielding is a good approximation to this data set, noting that ELM suppression was not present.

Single-fluid resistive modeling with the MARS-F code [23] (which permits imperfect shielding) is now used to demonstrate that the HFS response is primarily sensitive to the resonant currents while the LFS response is primarily sensitive to kink mode excitation. Figure 4 displays the key elements of the MARS-F response found using experimental profiles of resistivity and toroidal rotation, with two computations bracketing the experimental β_N range plotted. As with IPEC, synthetic probe modeling is found to reproduce the experimental $\Delta\phi_{UL}$ dependency, though the LFS magnitude [Fig. 4(a)] is again somewhat underpredicted. That MARS-F and IPEC find similar probe dependencies indicates that the imperfect shielding allowed by MARS-F is not contributing strongly to the measured trends.

Outputs of the MARS-F calculation directly related to kink mode excitation and to the total resonant field (including plasma response) are also shown [24]. Figure 4(d) illustrates

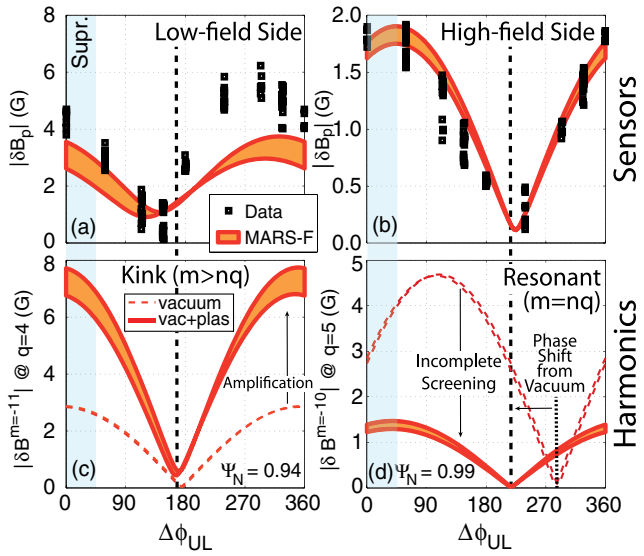

FIG. 4 (color online). [(a),(b)] Single-fluid resistive MHD modeling including flow (MARS-F) of the same data set. (c) Amplitude of the poloidal harmonic that is most amplified by the kink mode ($m > nq$), which is found to match the LFS response. (d) Amplitude of a resonant harmonic ($m = nq$), which is found to match the HFS response though only with the kink response included.

the dependence on $\Delta\phi_{UL}$ of a resonant harmonic ($m = nq$) at the pedestal foot ($q = 5$), where some penetration is computed. The resonant harmonic aligns well with the HFS data, though only if the plasma response is included. The computed resonant harmonics are thus not maximized when applied field is equilibrium-field aligned nor when kink amplification is maximized, but are instead somewhere in between. Note that the dependence of resonant harmonics farther into the pedestal (such as at $q = 4$) exhibit the same dependence on $\Delta\phi_{UL}$ as at $q = 5$. However, at $q = 4$ near-perfect shielding is predicted by MARS-F. Whether shielded or penetrated, MARS-F modeling of the $\Delta\phi_{UL}$ dependencies indicates that the HFS response is representative of the resonant currents. Because of the inverse major radius dependence of the toroidal field strength in a torus, most of an equilibrium field line's toroidal transits (per poloidal transit) occur on the HFS side, supporting the HFS response connection to the resonant currents, which must follow the field line.

Figure 4(c) shows the amplitude of the $m = -11$ harmonic at the $q = 4$ surface. This poloidal harmonic is well aligned with the kink mode structure ($m > nq$) and has the strongest amplification [25]. The dependence on $\Delta\phi_{UL}$ of this harmonic is found to be more closely aligned with the LFS array signal, displays a phase shift to lower $\Delta\phi_{UL}$ than both the vacuum and total resonant harmonic, and does not align with any global response. While the $q = 4$ surface is selected for analysis, identification of the most amplified harmonic can be done at any flux surface, and its dependence on $\Delta\phi_{UL}$ is invariant to the flux surface chosen.

Scans of β_N reinforce the connection of the pressure-driven kink excitation to the LFS sensors. Experimentally, a β_N ramp finds strong increases in the LFS response magnitude while the HFS is relatively unchanged, as shown in Fig. 5. For this scan a 0.5 kA fixed $\Delta\phi_{UL} = 0°$ $n = 2$ field is rotated at 20 Hz. The disparate dependency on β_N is reproduced with MARS-F modeling of these discharges (which differ slightly from those presented earlier as

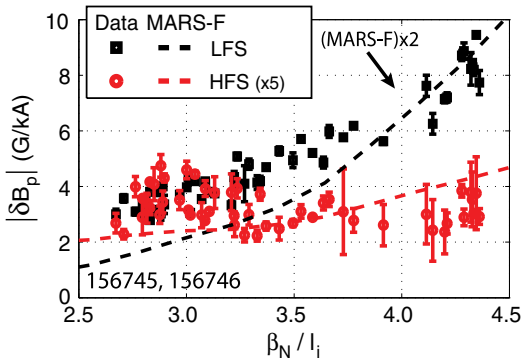

FIG. 5 (color online). Dependence of HFS and LFS plasma response as β_N is ramped, with internal inductance (l_i) normalization used. Experiment and MARS-F agree that the LFS response increases while the HFS response is relatively unaffected. The LFS magnitude is underpredicted.

$q_{95} = 4.3$ vs 4.1, and $\beta_n/l_i > 2.5$ vs ≈ 2.4) though the LFS response magnitude is again underpredicted. Within the MARS-F computation, the kink-amplified harmonics ($m > nq$) increase strongly with β_N, while the resonant harmonics ($m = nq$) are relatively unchanged. MARS-F also predicts that the LFS response null in $\Delta\phi_{\mathrm{UL}}$ is sensitive to β_N while the HFS null is invariant, though this remains to be confirmed.

Concluding remarks.—By continuously scanning $\Delta\phi_{\mathrm{UL}}$ (and thus the applied $n = 2$ poloidal spectrum) pumpout and ELM suppression have been shown to be coincident with maximized coupling to the HFS magnetic response, but not the LFS midplane response. The different $\Delta\phi_{\mathrm{UL}}$ dependence between the HFS and LFS midplane response directly measures the presence of multiple modes in the $n = 2$ response. Ideal and resistive MHD calculations reproduce these measurements and indicate that the HFS midplane response is correlated with the resonant (shielding) currents. The resonant currents are found to be maximized by applied fields that are not equilibrium field aligned. This is at least partly due to the effect of the pressure-driven kink mode of the plasma, which is correlated with the LFS measurement. The kink is found to be important to pumpout and ELM suppression through the modification of the resonant currents, which are in turn detected on the HFS. While these structures are identified as resonant currents and a kink mode, future work will investigate whether these results could also be described as two orthogonal eigenmodes of the ideal MHD equations, each with kinking and resonant components.

While a spectral study such as that presented herein cannot directly identify the mechanism responsible for pumpout and ELM suppression by the $n = 2$ field, this work has shown that both go like the HFS magnetic response and the shielded or penetrated resonant currents. The pumpout effect is shown to vary continuously with the HFS response and as such implicates resonant currents, either shielding inside of the pedestal or penetrated at the pedestal foot as these are all linearly proportional. For ELM suppression, this study is consistent with resonant currents increasing transport at the top of the pedestal, as suppression is found when resonant drive is maximized. While MARS-F finds the resonant fields are fully shielded, the brief ELM suppressed periods of Fig. 1 are coincident with bifurcations in the HFS sensors, T_e profile, and rotation profile, indicative of field penetration as discussed in a separate publication [26].

DIII-D data shown in this paper can be obtained in digital format by following the link in Ref. [27].

This material is based upon work supported by the U.S. Department of Energy, Office of Science, Office of Fusion Energy Sciences, using the DIII-D National Fusion Facility, a DOE Office of Science user facility, under Awards No. DE-FC02-04ER54698, No. DE-AC02-09CH11466, No. DE-FG02-04ER54761, No. DE-AC05-06OR23100, No. DE-SC0001961, and No. DE-AC05-00OR22725. S. R. H. was supported by AINSE and ANSTO.

*paz-soldan@fusion.gat.com

[1] A. Loarte *et al.*, Nucl. Fusion **47**, S203 (2007).
[2] T. E. Evans *et al.*, Phys. Rev. Lett. **92**, 235003 (2004).
[3] Y. M. Jeon *et al.*, Phys. Rev. Lett. **109**, 035004 (2012).
[4] W. Suttrop *et al.*, Phys. Rev. Lett. **106**, 225004 (2011).
[5] A. Kirk *et al.*, Nucl. Fusion **53**, 043007 (2013).
[6] Z. Unterberg *et al.*, Nucl. Fusion **50**, 034011 (2010).
[7] H. Reimerdes, M. Chu, A. Garofalo, G. Jackson, R. La Haye, G. Navratil, M. Okabayashi, J. Scoville, and E. Strait H. Reimerdes *et al.*, Phys. Rev. Lett. **93**, 135002 (2004).
[8] H. Reimerdes *et al.*, Nucl. Fusion **49**, 115001 (2009).
[9] M. J. Lanctot *et al.*, Phys. Plasmas **17**, 030701 (2010).
[10] R. A. Moyer, M. A. Van Zeeland, D. M. Orlov, A. Wingen, T. E. Evans, N. M. Ferraro, J. M. Hanson, R. Nazikian, M. R. Wade, and L. Zeng, Nucl. Fusion **52**, 123019 (2012).
[11] A. Wingen, N. M. Ferraro, M. W. Shafer, E. A. Unterberg, T. E. Evans, D. L. Hillis, and P. B. Snyder, Nucl. Fusion **54**, 064007 (2014).
[12] J.-K. Park, M. J. Schaffer, J. E. Menard, and A. H. Boozer, Phys. Rev. Lett. **99**, 195003 (2007).
[13] C. Paz-Soldan, R. J. Buttery, A. M. Garofalo, J. M. Hanson, R. J. La Haye, M. J. Lanctot, J. K. Park, W. M. Solomon, and E. J. Strait, Nucl. Fusion **54**, 073013 (2014).
[14] C. Paz-Soldan, M. J. Lanctot, N. C. Logan, D. Shiraki, R. J. Buttery, J. M. Hanson, R. J. La Haye, J.-K. Park, W. M. Solomon, and E. J. Strait, Phys. Plasmas **21**, 072503 (2014).
[15] M. J. Lanctot *et al.*, Nucl. Fusion **53**, 083019 (2013).
[16] S. R. Haskey, M. J. Lanctot, Y. Q. Liu, J. M. Hanson, B. D. Blackwell, and R. Nazikian, Plasma Phys. Controlled Fusion **56**, 035005 (2014).
[17] J. D. King *et al.*, Rev. Sci. Instrum. **85**, 083503 (2014).
[18] J.-K. Park, A. H. Boozer, and A. H. Glasser, Phys. Plasmas **14**, 052110 (2007).
[19] M. E. Fenstermacher *et al.*, Phys. Plasmas **15**, 056122 (2008).
[20] A. Kirk, Y. Liu, E. Nardon, P. Tamain, P. Cahyna, I. Chapman, P. Denner, H. Meyer, S. Mordijck, and D. Temple, Plasma Phys. Controlled Fusion **53**, 065011 (2011).
[21] A. H. Boozer, Fusion Sci. Technol. **59**, 561 (2011).
[22] Y. Liu, A. Kirk, Y. Gribov, M. P. Gryaznevich, T. C. Hender, and E. Nardon, Nucl. Fusion **51**, 083002 (2011).
[23] Y. Liu, A. Kirk, and E. Nardon, Phys. Plasmas **17**, 122502 (2010).
[24] S. R. Haskey, M. J. Lanctot, Y. Q. Liu, C. Paz-Soldan, J. D. King, B. D. Blackwell, and O. Schmitz, Plasma Phys. Controlled Fusion **57**, 025015 (2015).
[25] M. J. Lanctot *et al.*, Phys. Plasmas **18**, 056121 (2011).
[26] R. Nazikian *et al.*, Following Letter, Phys. Rev. Lett. **114**, 105002 (2015).
[27] See https://fusion.gat.com/global/D3D_DMP.